§SP-XXX-1

Mechanical Properties and Freezing and Thawing Behavior of 3D Printing Concrete containing Recycled Fine Aggregates from Construction and Demolition Waste

Yeakleang Muy[1], Luc Courard[1], Xavier Garnavault[1], David Bulteel[2,3], Sébastien Rémond[4], Maria Taleb[2,3], and Julien Hubert[1]

[1]University of Liege, Urban and Environmental Engineering, Building Materails, Quartier Polytech 1, Allée de la découverte 9, B-4000 Liège, Belgium
[2]IMT Nord Europe, Institut Mines-Telecom, centre of Materials and Processes, F-59000 Lille, France
[3]Univ. Lille, Institut Mines-Télécom, Univ. Artois, Junia, ULR 4515 - LGCgE – Laboratoire de Génie Civil et géoEnvironnement, F-59000 Lille, France
[4]Univ Orléans, Univ Tours, INSA CVL, LaMé, EA 7494, Rue Léonard De Vinci, 45072 Orléans, France

**Corresponding author: yeakleang.muy@uliege.be*

Synopsis: This study focuses on evaluating the mechanical, microstructural, and durability properties of 3D printing mortar (3DPM), with a specific emphasis on the influence of incorporating Recycled Fine Aggregates (RFA). These RFA are produced from Construction and Demolition Waste (C&DW) in Belgium and are sieved to a maximum particle size of 2 mm [0.08 in].

Cast and printed samples of mortar containing 100% RFA, with a sand-to-cement ratio of approximately 1:1 and a water-to-cement ratio of 0.29, were subjected to mechanical tests, including flexural, compressive, and tensile strength, at 2, 7, 28, and 56 days. The possible anisotropic behavior of the printed material was also investigated. The results show that using RFA does not significantly affect the mechanical properties of the mortar, and some anisotropic behavior was observed based on the compression test results. The end-goal of the project is to print non-reinforced urban furniture; in order to assess its durability, only freezing and thawing (F-T) behavior was investigated. The F-T behavior were analyzed based on the quantity of spalling particles after 7, 14, 28, 56, and 91 F-T cycles. The results show that up to 91 F-T cycles, no significant surface damage occurred.

Keywords: Construction and Demolition Waste, 3D printing concrete, durability of concrete, mechanical properties, Recycling

Yeakleang Muy is a post-doctoral researcher at the University of Liège in Belgium, affiliated with the Urban and Environmental Engineering unit. Her initial post-doctoral project is the INTERREG CIRMAP project, focusing on integrating recycled aggregate into the formulation of 3D printing mortar for shape customizing of urban furniture. In 2022, she earned her Ph.D. in Civil Engineering from INSA Rennes in France, focusing on the valorization of marine dredge sediment for partial cement substitution.

INTRODUCTION

In recent years, the construction industry has witnessed the development of a new building technology driven by innovations in additive manufacturing technologies, commonly referred to as 3D printing (3DP). Three-dimensional printing is a groundbreaking technique that involves the sequential printing of layers, one on top of the other. This method was first introduced in 1986 for prototyping purposes [1]. Compared with the traditional cast-in-situ concrete construction method 3D printing concrete construction presents several advantages such as the freedom of design, formwork-free fabrication, waste minimization and mass customization. [1- 4].

3D printing concrete (3DPC) is also being explored in the framework of the transition of the construction industry toward more sustainable and environmentally friendly building solutions [5, 6]. Indeed, the better material efficiency [4, 7] of this technology aligns with the global imperative to reduce the construction industry's carbon footprint and minimize waste generation. Yet, this technology is still facing important challenges linked to the important amount of cement and sand used in the process [8]. One promising avenue towards improving the environmental impact of 3DPC while promoting a circular economy is the incorporation of recycled materials into 3DPC formulations. The integration of Recycled Fine Aggregates (RFA) into concrete has been extensively studied due to its potential environmental benefits; however, its impact on the mechanical properties of concrete, including 3D Printed Concrete (3DPC), remains a topic of discussion. Several studies have highlighted the adverse effects of RFA on concrete's hardened properties, attributing them to RFA's lower density and higher water absorption [9]. Similar findings have been observed in the context of 3DPC, with Ding et al. reporting marginal decreases (up to 27%) in compressive strength but no clear influence on tensile and flexural strength with RFA substitution rates of up to 50% [10]. Moreover, Xiao et al. observed significant losses in mechanical performance, particularly in compressive strength (up to 48%), when using 100% recycled aggregates and sand [11]. This weakness can, in part, be addressed through fiber reinforcement, as demonstrated in Xiao's research [12].

RFA have, however, demonstrated potential in improving the buildability of 3DPC. Wu et al. and Xiao et al both conducted rheological, workability and buildability tests, noting faster decrease in workability but higher yield stress and faster shear modulus increase with increasing RFA substitution rate [12, 13]. These are both indicators of a better buildability. This is, once again, attributed to the higher water absorption of recycled concrete aggregates but also to their rougher surface compared to river sand. Similarly, Ding et al. reported accelerated early age strength development with RFA incorporation of up to 50%, suggesting enhanced buildability [14]. However, these benefits may come at the cost of a shortened printability window, posing challenges for large-scale applications [15]. Zou et al. proposed mitigating this issue by adding sodium gluconate to printing mortar containing recycled sand, extending the printability window while maintaining higher early-age strength compared to natural sand mortar limiting the strain in the bottom layer and therefore improving the overall buildability [15].

Despite extensive research on the mechanical aspects, the impact of RFA incorporation on the durability performance of 3DPC remains understudied [16]. This paper investigates the mechanical, microstructural, and durability properties of 3D printed mortar(3DPM) in which the natural sand has been substituted RFA. Specifically, in this study, natural quarry sand (crushed limestone) is being replaced by recycled fine concrete aggregates produced in the Tradecowall St-Ghislain recycling plant in Belgium. The materials have been characterized and mortar mixtures have been designed for both natural and recycled sands.

Comparative analyses are conducted, drawing distinctions between mortar samples containing RFA and those with natural sand. The investigation evaluates mechanical performance through flexural, compressive, and tensile strength tests. The changes in microstructure are assessed based on porosity, bulk density, and capillary absorption. The durability of the material is investigated via Freezing and Thawing (F-T) cycles resistance which is a crucial parameter for mortars and concrete-containing recycled materials. There is plenty of research which have been conducted on the F-T behavior of concrete [17-22] and mortar but for mortar, that is mostly for the masonry aspect.

The influence of the printing process itself is also studied and highlighted anisotropic behavior in printed mortar samples. Furthermore, the impact of curing methods on mortar properties is investigated because of the important amount of cement involved in 3DPC compositions.

MATERIALS AND METHODS

Materials

In this research, the fine aggregates obtained from the recycling of all-mixture concrete, denoted as recycled sand (RS), originate from the Tradecowall recycling center in St-Ghislain, Belgium. To ensure a ratio of at least 10 between the diameter of the printing nozzle and the largest grain size [19], the maximum grain size is restricted to 2 mm [0.08 in]. Recycled sand possesses a density of 2.39 tons/m^3 [149.21 lb/ft^3] and exhibits a water absorption rate of 5.31%.

The virgin aggregates employed as reference material, designated as natural sand (NS) within this research, were sourced from the Saint Bonnet quarry in France. The particle size distribution of the natural sand closely resembles that of the recycled sand, as illustrated in (Fig.1). This natural sand has a density of 2.62 tons/m^3 [163.56 lb/ft^3] and a water absorption capacity of 0.65%.

The portland cement employed is categorized as type CEMI 52.5N, procured from VICAT's manufacturing facility in Créchy, France. It functions as a hydraulic binder and possesses a density of 3.16 tons/m^3 [197.27 lb/ft^3].

The plasticizer Polycarboxylate (PCE) and the viscosity modifying admixture (VMA) used in this research were supplied by the company Chryso. These components play a crucial role in enhancing the workability of mortar, which in turn improves printability factors such as pumpability and extrudability, ultimately resulting in enhanced buildability (retaining capacity).

Mixture proportion and sample implementation

The mixtures proportions of the mortar used in the study are presented in Table 1. Two mortar formulations were employed for the tests: one featuring natural sand (NSM) and the other incorporating recycled sand (RSM). In the case of RSM, all the natural sand was substituted with recycled sand by mass. Additionally, the mixing water was adjusted to accommodate the higher water absorption of recycled sand, ensuring that the effective W_{eff}/C remained constant. In addition, both mortar NSM and RSM have similar workabilities based on the measurement of flow diameter following NBN EN 1015-3, which is equal to 125 mm [4.92 in] and 128 mm [5.04 in] respectively.

Cast samples

For laboratory fabricated cast samples, the mixing process begins with adding sand and water to the container, allowing them to pre-saturate for a duration of 300 seconds (no saturation step is required for the mixture with natural sand). Subsequently, cement, viscosity modifying agent, and superplasticizer are incorporated, and the mixture is blended for 30 seconds at low speed, followed by an additional 30 seconds at high speed. Following a brief 30 seconds pause, any mortar adhering to the container's walls is repositioned to the center during the mixing process. The sequence concludes by subjecting the mixture to high-speed mixing for 150 seconds. The implementation of these samples adhered to the guidelines specified in NBN EN 196-1 [20].

Printed samples

For printed samples, the cartesian printer shown in the Fig. 2(a) was used. The mixing procedure begins with mixing the first third of the materials, including sand, cement, and water, for a period of 2 min. This is followed by the inclusion of the second portion, in which the admixtures are added to the water, which is similarly mixed for 2 min. Lastly, the third portion is introduced and blended for an additional 11 min. Only the RSM formulation was utilized for the printing of elements. Specifically, "S"-shaped elements were continuously printed up to 6 layers as seen in Fig. 2(b).

Additionally, another "S"-shaped element, with the string distance adjusted to create a slab, was printed for subsequent freezing and thawing testing. After printing, these elements were covered with a plastic film and left for 48 h prior to controlled curing in a humid chamber (maintained at a relative humidity of 95 ± 5% and a temperature of 20 ± 2°C [68 ± 33.8°F]). The nomenclature RSM_C is employed for cast samples, while RSM_P is used for printed samples.

EXPERIMENTAL METHODS

Flow table test

The flow table test was conducted to access the workability of fresh mortar. This test was performed following the standard NBN EN 1015-3 and the flow diameter of both NSM and RSM mortar was measured.

Flexural and compressive strength test

Flexural and compressive strength evaluations were executed following the protocols outlined in the established standard NBN EN 196-1 [20]. Test prisms with dimensions of 40 × 40 × 160 mm³ [1.57 × 1.57 × 6.30 in³] were prepared and tested at intervals 2, 7, 28, 56 and 91 days.

For cast samples, they were manufactured and subsequently encased under plastic film for a 24 h period before demolding. Two groups of samples were created to assess the impact of curing conditions on the mortar. One group was cured underwater in a room with a temperature of 20 ± 3°C [68 ± 5.4°F] and a relative humidity exceeding 95% until the specified time. The second group underwent dry curing in a room with a temperature of 20 ± 3°C [68 ± 5.4°F] and a relative humidity of 60 ± 5%.

On the other hand, printed samples were extracted from the printed “S” element at each designated time and underwent testing from two distinct loading directions: parallel (oz) and perpendicular to the printing direction (ox), as shown in Fig. 3(b). The flexural test applied the load at a rate of 3 kN/min, while the compression test employed a loading rate of 144 kN/min. The flexural strength (R_f) and compressive strength (R_c) were then calculated based on the recorded failure load F_f and F, respectively, as shown in Eq. 1 and Eq. 2.

$$R_f = \frac{1.5 \times F_f \times l}{b^3} \qquad \text{Eq. 1}$$

$$R_c = \frac{F_c}{1600} \qquad \text{Eq. 2}$$

Where b is the side of the square section of the prism (mm), F_f is the maximum load until failure, applied to the middle of the prism (N), l is the distance between the support (mm), F_c is the maximum load until failure, applied to the surface of 40 × 40 mm² [1.57 × 1.57 in²] of two half prisms resulted from flexural test (N), and *1600* is the area of the platens or auxiliary plates 40 × 40 mm² [1.57 × 1.57 in²] (mm²).

Tensile strength test

Tensile strength was evaluated following the guidelines outlined in the established standard NBN B15-211 [22]. Cylindrical specimens, measuring 50 mm [1.97 in] in diameter and 50 mm [1.97 in] in height, were prepared and tested at intervals of 7, 28, 56 and 91 days for cast samples and exclusively at 91 days for printed samples. The cast samples were drilled from cubic specimens of dimensions of 150 × 150 × 150 cm³ [59.06 × 59.06 × 59.06 in³]. On the other hand, the printed samples were drilled perpendicularly to the printed layers from the printed “S” shape element. The outline of the layers was then traced approximately based on the visible interface on the printed element, as depicted in Fig. 4(a). The experimental procedure was executed using INSTRON instrument as shown in Fig. 4(b) with a pulling rate set at 0.10 ± 0.05 MPa/s [14.50 ± 7.25 psi/s]. The tensile strength (R_t) was also calculated based on its failure load F_t, as shown in Eq. 3.

$$R_t = \frac{F_t}{S} \qquad \text{Eq. 3}$$

Where F_t is the maximum load using until the rupture of mortar (N), and S is the section of the fracture surface (mm^2).

Porosity and bulk density measurements

Porosity ε and bulk density ρ_d of the mortar were evaluated in accordance with standard NF P18-459 [11]. Cube-shaped samples, measuring 40 x 40 x 40 mm³ [1.57 × 1.57 × 1.57 in^3], were employed for these measurements and for both cases of cast and printed samples. The assessment was conducted at specific time intervals: 2, 7, 28, 56, and 91 days. The procedure involved placing the samples under vacuum conditions for a duration of 4 ± 0.5 h, followed by saturation under vacuum for an additional 44 ± 1 h. After saturation, the test samples were gently dried by removing excess surface water with a damp cloth and then weighed (m_1). Subsequently, hydrostatic weighing was performed (m_2) and finally, all the samples were placed in an oven and dried at 60°C [140°F] until a constant mass was attained (m_3). The formulas to calculate the mortar's porosity and bulk density are provided in Eq. 4, and Eq. 5 respectively.

$$\varepsilon = \frac{m_1 - m_3}{m_1 - m_2} \times 100 \qquad \text{Eq. 4}$$

$$\rho_d = \frac{m_3}{m_1 - m_2} \times \rho_w \qquad \text{Eq. 5}$$

Where ρ_w is the water density (kg/m^3)

Capillary absorption measurement

The capillary water absorption assessment was executed utilizing the suction method adapted from the established standard NBN EN 13057 [24]. Prism samples with dimensions of 40 × 40 × 160 mm³ [1.57 × 1.57 × 6.30 in^3] were employed for this examination, whether they originated from cast or printed samples. Following a 28-day curing period, all specimens underwent a 1 cm [0.39 in] cut on the testing surface to ensure consistent surface conditions. They were, then, dried in an oven set at 40 ± 2°C [104 ± 3.6°F] for 7 days, and the weight stability was ensure by verifying a mass loss of less than 0.2% after two successive weighings with a 2-hour interval. According to the specifications of the standard NBN EN 13057 [24], the tested specimens were submerged in a tank containing demineralized water, with the tested surface immersed to a depth of 2 ± 1 mm [0.08 ± 0.04 in], facilitated by a small pins holder. The tank was sealed with a lid. The amount of water absorbed by the samples was determined through successive weighing at various time intervals: 12 min, 30 min, 1 h, 2 h, 4 h, 5 h, and 24 h. The water uptake per unit area, *i*, was calculated for each time increment from the absorbed weight of water divided by surface area of the of the specimen in contact with the water. However, it is important to note that this method does not ensure unidirectional absorption. To verify this condition, two sets of samples were investigated: one set remained untreated while the other wascoated with epoxy resin. The absorption was also evaluated in two directions: (oz) and (ox) for both cast and printed specimens. In this case, for cast specimens, (oz) direction refers to the bottom and (ox) direction refers to the side surface of specimens.

Freezing and thawing test

The freezing and thawing test adhered to the standard RNR 50-1 [25], which is based on CEN/TS 12390-9 [26]. For this experiment, cylindrical specimens were prepared, featuring a diameter of 113 mm [4.45 in] and a height of 50 ± 2 mm [1.97 in ± 0.08 in]. In the case of cast samples, the specimens with dimensions of 150 x 150 x 150 mm³ [5.91 × 5.91 × 5.91 in^3] were initially cured for 28 days before drilling to obtain two cylindrical specimens from each cube. For the printed samples, the printed slab also underwent 28 days of curing before drilling to obtain the desired dimensions. After curing, all samples were exposed to an environment with a temperature of 20 ± 3°C [68 ± 5.4°F] and a relative humidity of 60 ± 5% for 14 days before being prepared (approximately 3 days) and tested. The freezing and thawing cycle adopted for the test was between -20°C [-4°F] and 20°C [68°F] as depicted in Fig. 5. To assess freezing and thawing resistance, the mass of spalling particles from the test surface was measured after 7, 28, 56, and 91 freezing and thawing cycles.

The evaluation of freezing and thawing resistance was carried out under three distinct surface conditions, with four samples for each condition:

- No solution (NS) - Only the surface was saturated.
- Water solution (WS) - The surface was covered with 3 mm [1.19 in] of demineralized water.
- Saline solution (SS) - The surface was covered with 3 mm [1.19 in] of saline solution (3% NaCl).

These surface conditions were chosen to simulate the different levels of severity in the environmental conditions which showing the most severe conditions exposed to the freezing and thawing phenomenon.

RESULTS AND DISCUSSION

Effect of sand replacement and printing method on mechanical and microstructural properties

The results regarding the flexural and compressive strengths of cast mortar samples containing recycled sand (RSM_C) and natural sand (NSM_C) are visually represented in Fig. 6. In Fig. 6(a), it can be observed that the flexural strength of RSM_C varied from 7.6 to 10.5 MPa [1102.29 to 1522.896 psi], while NSM_C exhibited a range of 9.3 to 12.9 MPa [1348.85 to 1870.987 psi]. In general, the flexural strength of RSM_C reached between 63.1% and 79.8% of that of NSM_C, except for the 7-day result. Importantly, statistical analysis using Student's t-distribution did not reveal any significant differences in these results.

Conversely, the findings related to compressive strength indicated a slight decrease in the strength of RSM_C compared to that of NSM_C when the water content was kept constant, as depicted in Fig. 6(b). As expected, the compressive strength showed an overall increase with time. The strength values ranged from 52.5 to 85.1 MPa [7614.48 to 12342.71 psi] for RSM_C and from 61.3 to 89.9 MPa [8890.81 to 13038.89 psi] for NSM_C, respectively. Notably, the compressive strength of RSM_C reached approximately 85.7% to 101% of that of NSM_C, with the 28-day result reaching 101%.

Fig. 7 illustrates the findings regarding the capillary absorption of cast specimens RSM_C and NSM_C. These results confirm that the change in sand type does not have a significant impact on the capillary system. Specifically, at 24 h of absorption, all mortar samples absorbed a mass of water ranging from 0.65 to 0.75 kg/m^2 [0.13 to 0.15 lb/ft^2], as shown in Fig. 7(a). The coefficient of absorption for the mortar was analyzed through linear regression, yielding values ranging from 0.168 to 0.191 $kg/m^2.h^{0.5}$ [0.03 to 0.04 $lb/ft^2.h^{0.5}$], with R^2 values falling between 0.845 and 0.854, as illustrated in Fig. 7(b). Notably, the RSM_C specimens appear to exhibit greater homogeneity than the NSM_C specimens, as their coefficient of absorption values are closely clustered in all absorption directions.

Effect of curing method on development of mechanical and microstructural properties

Fig. 8 presents the flexural and compressive strength of RSM_C under two different curing conditions such as water curing and ambient (at 60% RH) curing.

In general, it appears that the curing method does not have a significant impact on flexural strength. However, there is a noticeable drop in flexural strength at 2 days, which can be attributed to the loss of water necessary for the hydration process. After 7 days of curing, the positive influence of water curing on hydration reactions becomes evident, as depicted in Fig. 8(a).

In contrast, when it comes to compressive strength, ambient curing results in a significant decrease in strength, even at later stages, as shown in Fig. 8(b). This decline is likely attributed to the early loss of water, which promotes the development of shrinkage and micro-cracks. This distinction is particularly prominent in the case of the studied cementitious ink due to the substantial amount of cement in its formulation.

When comparing the compressive strength of mortar RSM_C cured in ambient conditions to the water-cured mortar described in the previous section, the compressive strength of the mortar cured in an ambient environment reached only 60.3% of those cured in water at 28 days, with almost no significant evolution observed beyond 7 days of curing due to a poor hydration reaction.

Anisotropy of compressive strength

Fig. 9 presents the results of compressive strength tests conducted on printed mortars in two loading directions, namely RSM_P (oz) and RSM_P (ox), in comparison to cast mortars RSM_C. In general, the compressive strengths of the printed samples are lower than those of the cast samples, primarily due to differences in the processing methods. For instance, at the 28-day mark, the compressive strength of the printed mortar differs from that of the cast mortar by approximately 35% for the RSM_P (oz) orientation and approximately 16% for the RSM_P (ox) orientation.

Moreover, regarding the anisotropy of compressive strength, the results also indicate that printed mortars exhibit greater strength in the (ox) orientation. This observation aligns with prior research by various authors [21], [27], [28], as cited in the review by Rehman and Kim [129]. This phenomenon can be attributed to a less dense zone outside the compression region of RSM_P (oz) samples compared to that of RSM_P (ox) samples. This less dense zone is created during the printing because the layer being printed is “pushed” in the previous layer to widen them to obtain layers that are at least 6 cm [2.36 in] wide while printing with a 2 cm [0.79 in] nozzle.

Bond strength properties of 3D printing mortar

The Table 2 presents the tensile strength values and the corresponding failure patterns for the printed specimens RSM_P. The average tensile strength falls within the range of 2.03 to 2.69 MPa [294.43 to 390.15 psi]. Notably, the observed failures did not occur between layers; instead, they seemed to manifest randomly, as depicted in both Table 2 and Fig. 10. This observation suggests the potential homogeneity of the mixture, possibly attributable to the layer compression applied during the printing process. Additionally, it's worth noting that the mixture composition did not include a setting time accelerator, which might have contributed to these outcomes.

These findings align with the results obtained from the compression tests. If the material had interfaces or weak planes between the layers, one would expect a lower compressive strength in the RSM_P (ox) direction compared to the other direction, influenced by the Poisson’s ratio. However, this was not observed, further supporting the conclusion of material homogeneity.

Effect of printing method on microstructural properties of mortar

The Fig. 11(a) and Fig. 11(b) highlight the porosity and bulk density of cast and printed mortars at various time periods. In general, the porosity of the mortar ranged between 17.71% and 21.07%, with a decrease in porosity observed over time. For RSM_C mortar, the porosity decreased by 0.39% from 21.07% after 2 days of curing to 20.68% after 56 days of curing. In the case of NSM_C mortar, the porosity decreased by 1.66% from 19.37% after 2 days of curing to 17.71% after 56 days of curing.

However, it's worth noting that the bulk density of NSM_C mortar is significantly higher than that of both the recycled sand mortar, RSM_C, and RSM_P. As expected, the porosity of NSM_C is also lower than that of RSM_C. The printing process tends to create a denser microstructure in the mortar compared to conventional casting. The results of capillary absorption, as shown in Fig.12, also confirm this observation, with RSM_P mortar exhibiting the lowest water absorption.

Effect of tested surface size and coating preparation on the capillary absorption of mortar

Fig. 13 illustrates the impact of epoxy resin covering on the capillary absorption properties of cast mortar. The results make it evident that the smaller the absorption surface, the more significant the effect of the coating. For instance, the non-coated sample RSM_C, exhibits much higher water absorption in the (oy) direction, where the contact surface is 1600 mm^2 [2.48 in^2] than in the other two directions. However, after coating, the water absorption becomes similar in all directions. In the case of samples with a contact surface of 6400 mm^2 [9.92 in^2], a slight difference is observed between coated and non-coated samples in all absorption directions. These findings emphasize the importance of selecting the appropriate surface size for testing the absorption of printed specimens.

Freezing and thawing behavior of mixture proportions

Fig. 14 shows the outcomes of the freezing and thawing test following exposure to 91 freezing and thawing cycles under three distinct surface conditions. Overall, the results indicate that the specimens' surfaces experienced minimal damage after undergoing 91 freezing and thawing cycles, whether the mortar was cast or printed. The cumulative spalling particles after 91 freezing and thawing cycles were found to be less than 1 g/m^2 [0.0002 lb/ft^2]. This resilience can be attributed to the favorable matrix of the mortar, which inherently contains micro-pores that are less susceptible to frost-related damage. A similar outcome was observed by Algourdin et al. [30], where no significant surface damage was detected in recycled sand-based mortar, even after subjecting it to 96 freezing and thawing cycles.

Furthermore, the results reveal that different saturation surface conditions had varying effects on the freezing and thawing test. Using a salt solution was found to create the most severe environment for the freezing and thawing test, followed by using a water solution on the surface. The least severe condition was observed when no solution was applied to the surface, and only saturation was performed, as depicted in Fig. 14(a).

CONCLUSION

This comprehensive research study has shed light on several crucial aspects pertaining to 3D-printed mortar, particularly in the context of incorporating Recycled Fine Aggregates (RFA) in substitution to natural sand :

- The research showed that replacing natural sand with RFA did not significantly impact the mechanical properties of the mortar. Both mechanical performances and microstructural characteristics exhibited similar trends for mortars containing RFA and those with natural sand. This suggests that RFA can be a viable and sustainable alternative in 3D-printed mortar without compromising mechanical performances.
- An interesting finding was the anisotropic behavior observed in 3D-printed mortar samples. The compressive strength of printed mortar varied depending on the loading direction, with the perpendicular direction (RSM_P (ox)) exhibiting higher strength. Direct tensile tests showed that failures occurred randomly within the material rather than at the interfaces between printed layers. These observations challenge conventional assumptions about the existence of a weaker interface between layers of 3D-printed materials and highlights the need for further research.
- The study assessed the freezing and thawing resistance of the mortar, usually a limiting factor for concretes and mortars produced with recycled aggregates. Remarkably, both cast and printed mortars demonstrated excellent freezing and thawing resistance, with minimal surface damage even after 91 freeze-thaw cycles. This resilience is attributed to the favorable matrix of the mortar, which contains micro-pores that are less susceptible to frost-related damage.
- The curing method employed showed significant influence on the mechanical properties of the mortar. Ambient curing led to important decrease in mechanical performances underscoring the importance of appropriate curing conditions for 3D-printed mortar due to the important amount of cement involved.

These results show that RFA can be used in 3D-printed mortar without compromising mechanical or durability properties. The study also highlights the complexity of 3D printing processes, including anisotropic behavior and the need for careful consideration of curing methods.

ACKNOWLEDGEMENT

The authors extend their gratitude to the Interreg North-West Europe program for providing funding for this research within the framework of the CIRMAP project.

REFERENCES

[1] M. D. Cohen, Y. Zhou, and W. L. Dolch, "Non-Air-Entrained High-Strength Concrete--Is it Frost Resistant?," *MJ*, vol. 89, no. 4, pp. 406–415, Jul. 1992, doi: 10.14359/2582.

[2] G. Fagerlund, "FROST RESISTANCE OF HIGH PERFORMANCE CONCRETE- SOME THEORETICAL CONSIDERATIONS," 1994.

[3] R. Zaharieva, F. Buyle-Bodin, and E. Wirquin, "Frost resistance of recycled aggregate concrete," *Cement and Concrete Research*, vol. 34, no. 10, pp. 1927–1932, Oct. 2004, doi: 10.1016/j.cemconres.2004.02.025.

[4] Ngo, T. D., Kashani, A., Imbalzano, G., Nguyen, K. T., & Hui, D. (2018). Additive manufacturing (3D printing): A review of materials, methods, applications and challenges. Composites Part B: Engineering, 143, 172-196.

[5] Zhao, Z., Ji, C., Xiao, J., Yao, L., Lin, C., Ding, T., & Ye, T. (2023). A critical review on reducing the environmental impact of 3D printing concrete: Material preparation, construction process and structure level. Construction and Building Materials, 409, 133887.

[6] Han, Y., Yang, Z., Ding, T., & Xiao, J. (2021). Environmental and economic assessment on 3D printed buildings with recycled concrete. Journal of Cleaner Production, 278, 123884.

[7] Damineli, B. L., Kemeid, F. M., Aguiar, P. S., & John, V. M. (2010). Measuring the eco-efficiency of cement use. Cement and Concrete Composites, 32(8), 555-562.

[8] Zhang, C., Nerella, V. N., Krishna, A., Wang, S., Zhang, Y., Mechtcherine, V., & Banthia, N. (2021). Mix design concepts for 3D printable concrete: A review. *Cement and Concrete Composites*, *122*, 104155.

[9] Dapena, E., Alaejos, P., Lobet, A., & Pérez, D. (2011). Effect of recycled sand content on characteristics of mortars and concretes. *Journal of Materials in Civil Engineering*, *23*(4), 414-422.

[10] Ding, T., Xiao, J., Zou, S., & Wang, Y. (2020). Hardened properties of layered 3D printed concrete with recycled sand. *Cement and Concrete Composites*, *113*, 103724.

[11] Xiao, J., Lv, Z., Duan, Z., & Hou, S. (2022). Study on preparation and mechanical properties of 3D printed concrete with different aggregate combinations. *Journal of Building Engineering*, *51*, 104282.

[12] Xiao, J., Zou, S., Ding, T., Duan, Z., & Liu, Q. (2021). Fiber-reinforced mortar with 100% recycled fine aggregates: A cleaner perspective on 3D printing. *Journal of Cleaner Production*, *319*, 128720.

[13] Wu, Y., Liu, C., Liu, H., Zhang, Z., He, C., Liu, S., ... & Bai, G. (2021). Study on the rheology and buildability of 3D printed concrete with recycled coarse aggregates. *Journal of Building Engineering*, *42*, 103030.

[14] Ding, T., Xiao, J., Qin, F., & Duan, Z. (2020). Mechanical behavior of 3D printed mortar with recycled sand at early ages. *Construction and Building Materials*, *248*, 118654.

[15] Zou, S., Xiao, J., Ding, T., Duan, Z., & Zhang, Q. (2021). Printability and advantages of 3D printing mortar with 100% recycled sand. *Construction and Building Materials*, *273*, 121699.

[16] Martínez-García, R., de Rojas, M. S., Jagadesh, P., Lopez-Gayarre, F., Morán-del-Pozo, J. M., & Juan-Valdes, A. (2022). Effect of pores on the mechanical and durability properties on high strength recycled fine aggregate mortar. *Case Studies in Construction Materials*, *16*, e01050.

[17] M. Pigeon, J. Marchand, and R. Pleau, "Frost resistant concrete," *Construction and Building Materials*, vol. 10, no. 5, pp. 339–348, Jul. 1996, doi: 10.1016/0950-0618(95)00067-4.

[18] M. Pigeon, R. Gagné, P.-C. Aïtcin, and N. Banthia, “Freezing and thawing tests of high-strength concretes,” *Cement and Concrete Research*, vol. 21, no. 5, pp. 844–852, Sep. 1991, doi: 10.1016/0008-8846(91)90179-L.

[19] K. El Cheikh, S. Rémond, N. Khalil, and G. Aouad, “Numerical and experimental studies of aggregate blocking in mortar extrusion,” *Construction and Building Materials*, vol. 145, pp. 452–463, Aug. 2017, doi: 10.1016/j.conbuildmat.2017.04.032.

[20] NBN EN 196-1, “Méthode d’essais des ciments - Partie1: Détermination des résistances.” 2016. Accessed: May 19, 2023. [Online]. Available: https://www.nbn.be/data/r/platform/frontend/detail?p40_id=174469&p40_language_code=nl&p40_detail_id=78149&session=0

[21] R. J. M. Wolfs, F. P. Bos, and T. A. M. Salet, “Hardened properties of 3D printed concrete: The influence of process parameters on interlayer adhesion,” *Cement and Concrete Research*, vol. 119, pp. 132–140, May 2019, doi: 10.1016/j.cemconres.2019.02.017.

[22] NBN B 15 211, “Concrete testing - Direct tensile strength.” 1974. Accessed: May 21, 2023. [Online]. Available: https://shop.standards.ie/en-ie/standards/nbn-b-15-211-1974-740821_saig_nbn_nbn_1798581/

[23] NF P18-459, “Essai pour béton durci - Essai de porosité et de masse volumique,” p. 9p, Mar. 2010.

[24] NBN EN 13057, “Products and systems for the protection and repair of concrete structures - test methods - determination of resistance of capillary absorption.” 2002. Accessed: May 22, 2023. [Online]. Available: https://shop.standards.ie/en-ie/standards/nbn-en-13057-2002-763729_saig_nbn_nbn_1844397/

[25] RNR 50-1 (3.0), “Note réglementaire pour fiches techniques, notes justicatives et études préliminaires du béton routier | COPRO.” Accessed: Jan. 27, 2023. [Online]. Available: https://www.copro.eu/en/document/rnr-50-1-30-note-reglementaire-pour-fiches-techniques-notes-justicatives-et-etudes

[26] CEN/TS 12390-9, “Testing hardened concrete - Part 9: Freeze-thaw resistance with de-icing salts - Scaling,” p. 10p, 2016.

[27] G. Ma, Z. Li, L. Wang, F. Wang, and J. Sanjayan, “Mechanical anisotropy of aligned fiber reinforced composite for extrusion-based 3D printing,” *Construction and Building Materials*, vol. 202, pp. 770–783, Mar. 2019, doi: 10.1016/j.conbuildmat.2019.01.008.

[28] V. Mechtcherine *et al.*, “Extrusion-based additive manufacturing with cement-based materials – Production steps, processes, and their underlying physics: A review,” *Cement and Concrete Research*, vol. 132, p. 106037, Jun. 2020, doi: 10.1016/j.cemconres.2020.106037.

[29] A. U. Rehman and J.-H. Kim, “3D Concrete Printing: A Systematic Review of Rheology, Mix Designs, Mechanical, Microstructural, and Durability Characteristics,” *Materials*, vol. 14, no. 14, p. 3800, Jul. 2021, doi: 10.3390/ma14143800.

[30] N. Algourdin, Q. N. A. Nguyen, Z. Mesticou, and A. Si Larbi, “Durability of recycled fine mortars under freeze-thaw cycles,” *Construction and Building Materials*, vol. 291, May 2021, doi: 10.1016/j.conbuildmat.2021.123330.

Table 1—Mixtures proportions of mortars (kg) [1 kg = 2.20 lbs]

	Cement	Sand	Water	Plasticizer	VCA	W_{eff}/C
RSM/NSM	905,00	995,60	313,52	22,63	1,81	0,29

Table 2—Tensile strength and failure pattern of printed specimens RSM_P

	Tensile strength MPa [psi]	**Failure pattern* mm [in]**	**Average tensile strength MPa [psi]**
7 days	2.02 [292.98]	28 to 34 [1.10 to 1.34]	
	2.14 [310.38]	13 to 25 [0.51 to 0.98]	2.03 ± 0.11 [294.43 ± 15.95]
	1.92 [278.47]	18 to 30 [0.71 to 1.18]	
28 days	2.71 [393.05]	12 to 16 [0.47 to 0.63]	
	2.52 [365.50]	18 to 25 [0.71 to 0.98]	2.51 ± 0.20 [364.04 ± 29.00]
	2.32 [336.49]	18 to 27 [0.71 to 1.06]	
56 days	2.43 [352.44]	17 to 28 [0.67 to 1.10]	
	3.03 [439.46]	20 to 33 [0.79 to 1.30]	2.69 ± 0.31 [390.15 ± 44.96]
	2.60 [377.10]	23 to 33 [0.91 to 1.30]	
91 days	2.28 [330.69]	26 to 32 [1.02 to 1.26]	
	2.11 [306.03]	17 to 31 [0.67 to 1.22]	2.25 ± 0.13 [326.33 ± 18.85]
	2.37 [343.74]	19 to 27 [0.75 to 1.06]	

*The failure pattern was measured from the top of the specimens

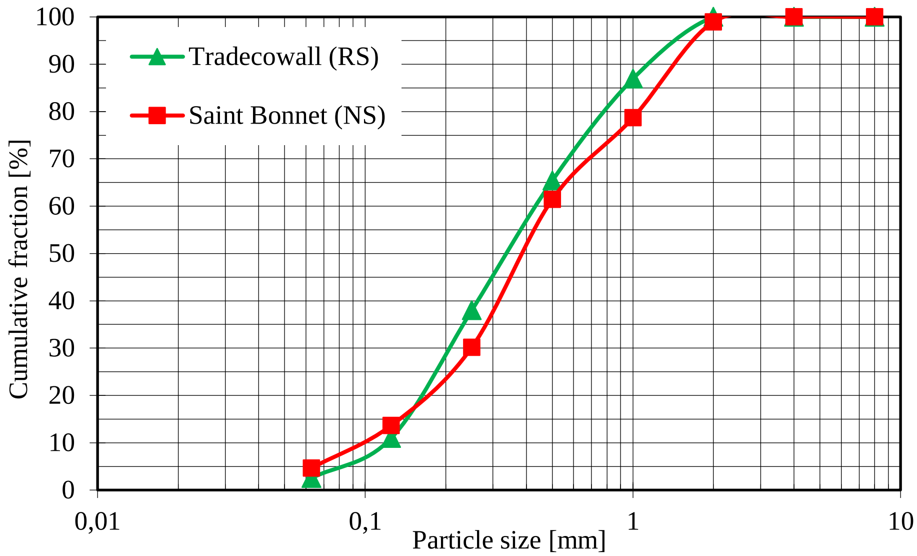

[1 mm = 0.0394 in]

Fig. 1—Particle size distribution curve of recycle sand, Tradecowall (RS), and natural sand, Saint Bonnet (NS)

(a) (b)

Fig. 2—Cartesian printer of IMT Nord Europe (a) and the printed element in « S » shape (b)

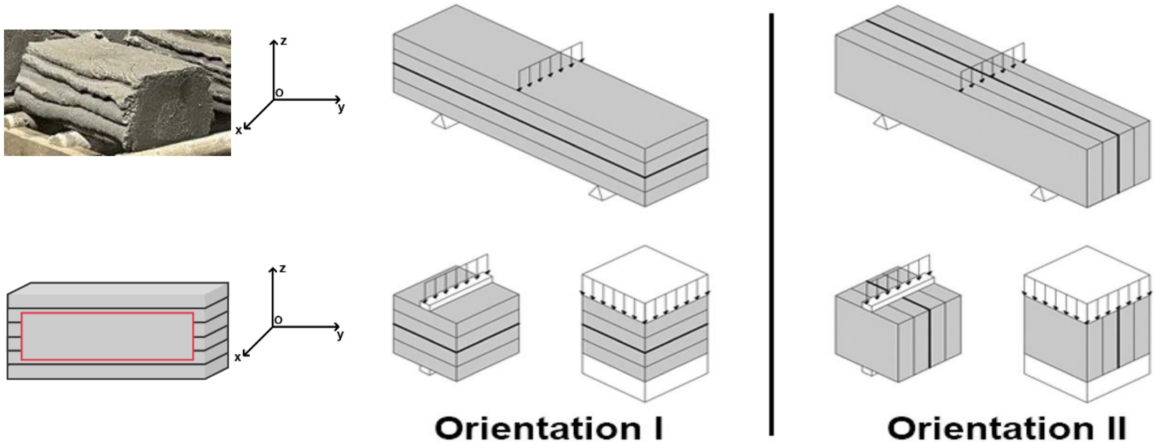

(a) (b)

Fig. 3—Schematic depicting the printed sample and the illustration of the sampling (a), along with the various orientations of load application on the samples [9] (b)

(a) (b)

Fig. 4—Cored of printed samples (a) and the INSTRON instrument using for tensile strength test (b)

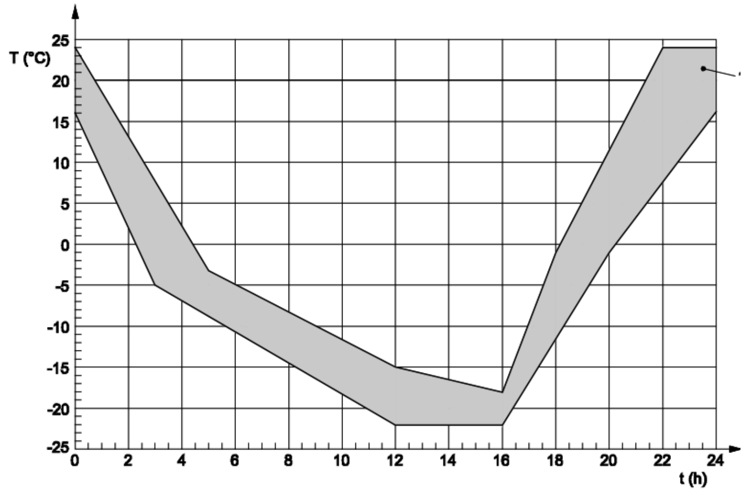

[(1°C × 9/5) + 32 = 33.8°F]

Fig. 5— Target temperature range for each freezing and thawing test cycle [14]

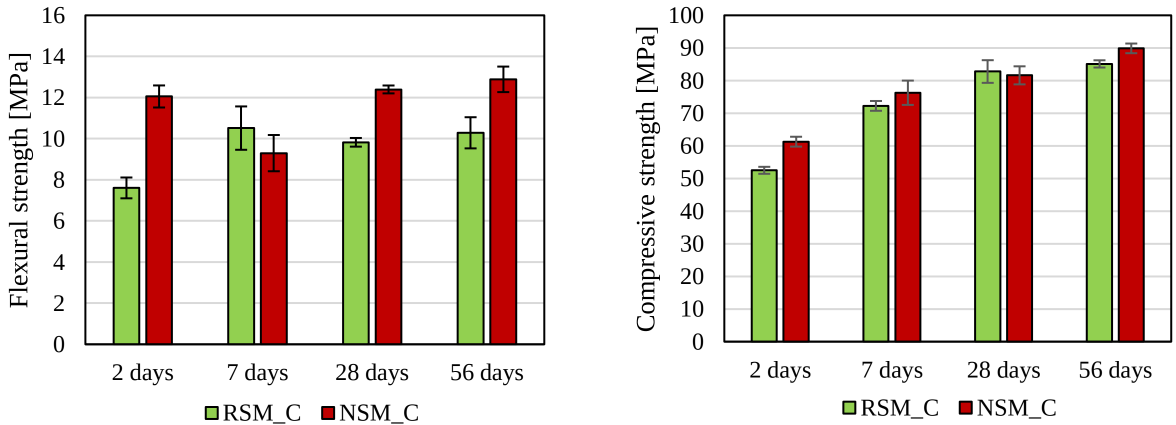

(a) (b)

[1 MPa = 145.04 psi]

Fig. 6—Flexural (a) and compressive strength (b) of cast mortar containing recycled sand RSM_C and natural sand NSM_C underwent water curing

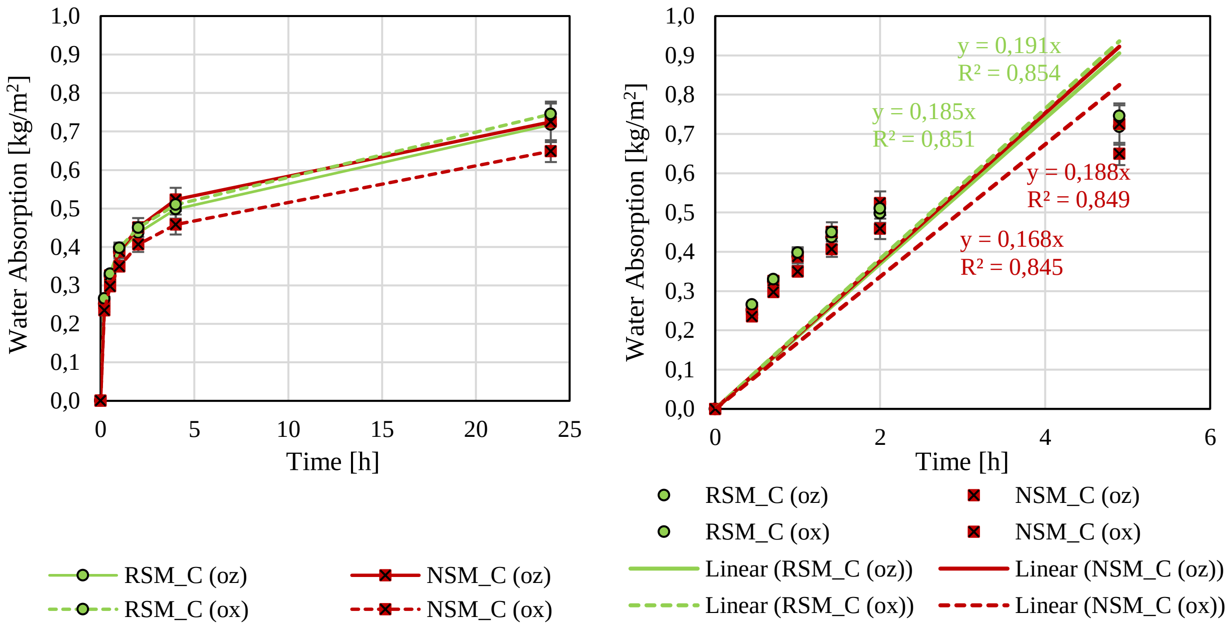

(a) (b)

[1 kg/m^2 = 0.2048 lb/ft^2]

Fig. 7—Amount of water absorbed per unit area (a) and the water absorption coefficient (b) for cast mortar samples containing recycled sand RSM_C and natural sand NSM_C in two orientations, namely (oz) and (ox), after 24 h of absorption.

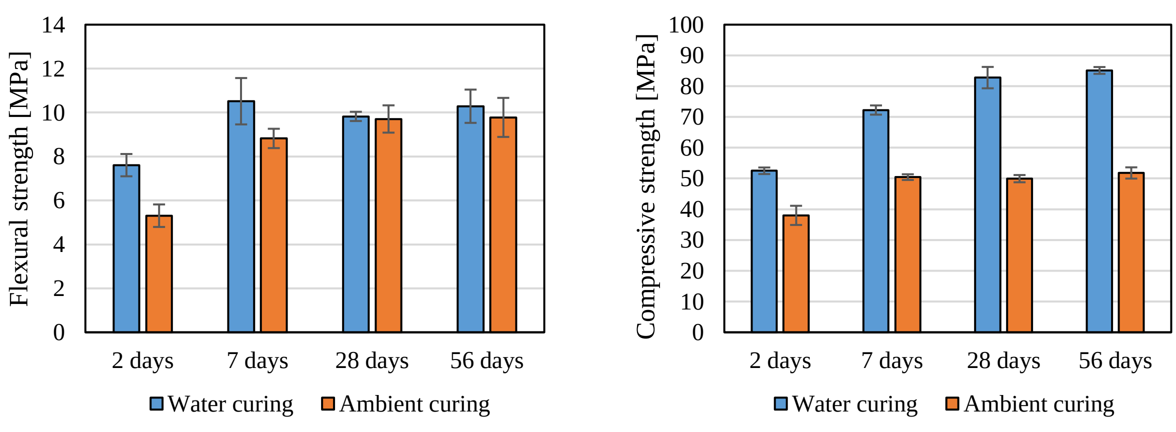

(a) (b)

[1 MPa = 145.04 psi]

Fig. 8—Flexural (a) and compressive strength (b) of cast mortar with recycled sand under water curing and ambient curing

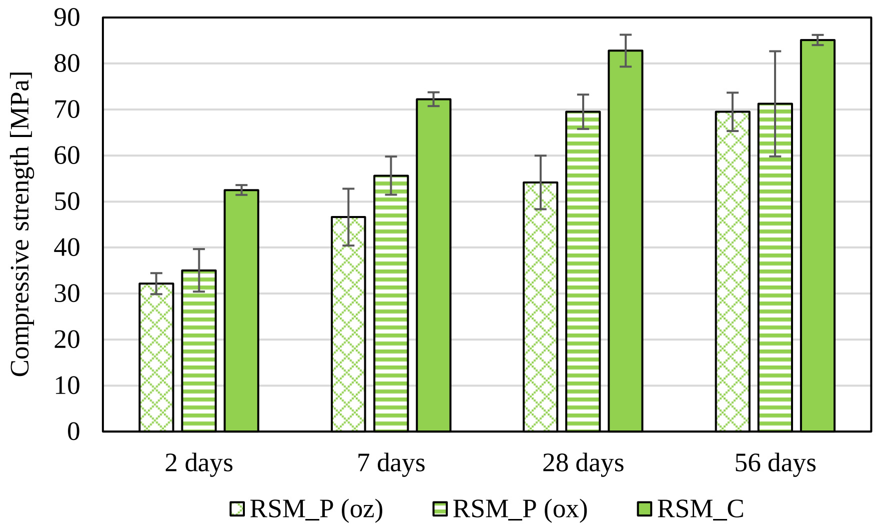

[1 MPa = 145.04 psi]

Fig. 9—Compressive strength of printed mortar specimens which the layer parallel to loading direction RSM_P (oz), the layer perpendicular to loading direction RSM_P (ox), and cast mortar RSM_C

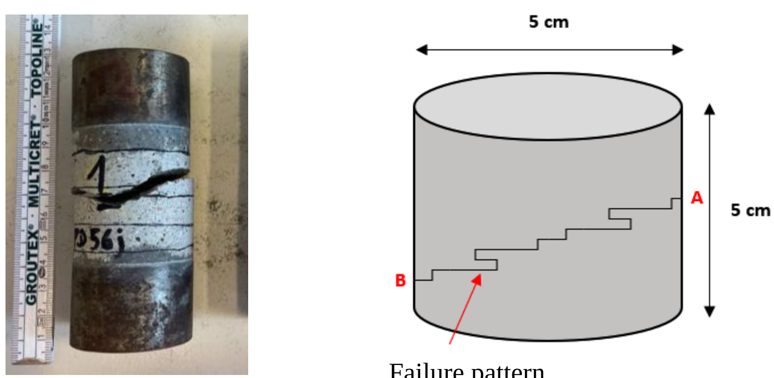

(a) (b)

[1 cm = 0.3937 in]

Fig. 10—Failure pattern of printed specimens after tensile test

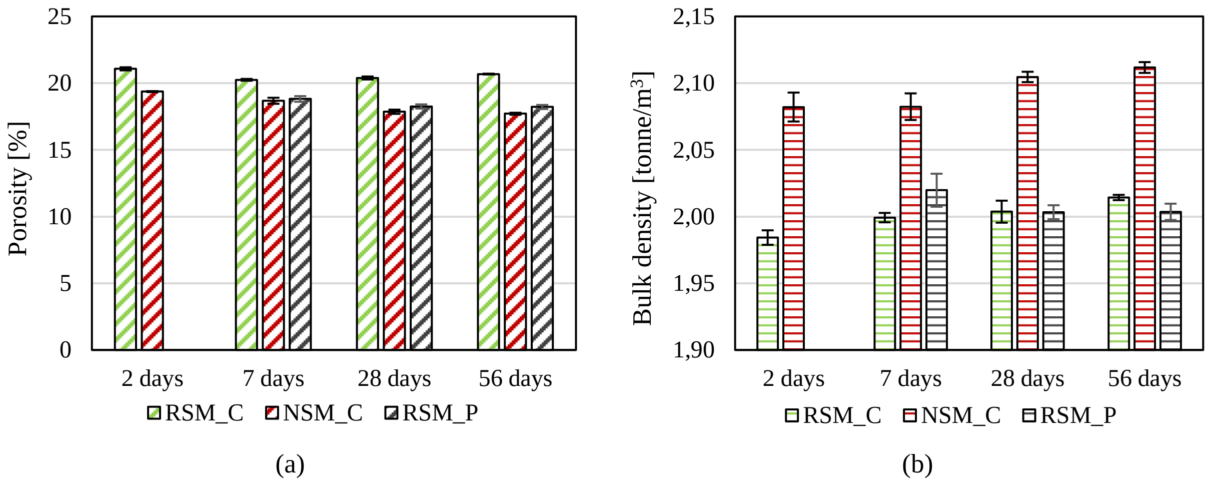

[1 tonne/m^3 = 62.43 lb/ft^3]

Fig. 11—Porosity (a) and bulk density (b) of cast and printed specimens underwent water curing

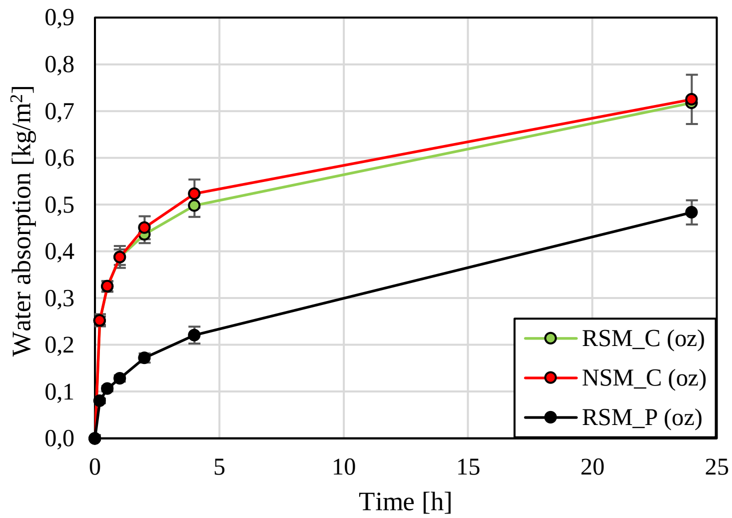

[1 kg/m^2 = 0.2048 lb/ft^2]

Fig. 12—Amount of water absorbed per unit area of cast mortar RSM_C and NSM_C and printed mortar RSM_P along the (oz) orientation

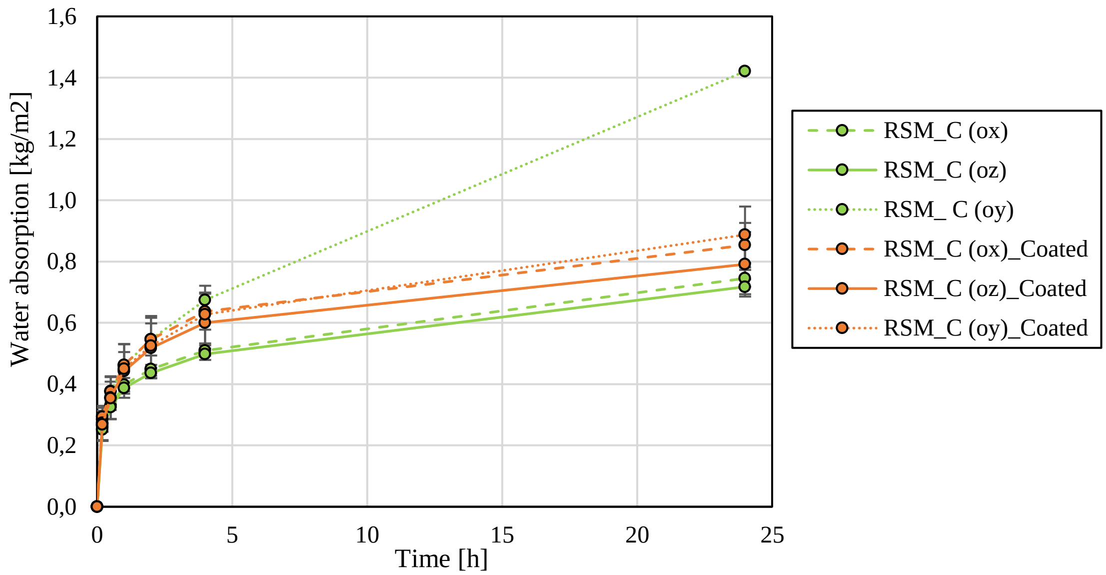

[1 kg/m^2 = 0.2048 lb/ft^2]

Fig. 13—Effect of covering specimens by epoxy resin on the capillary absorption properties of cast mortar

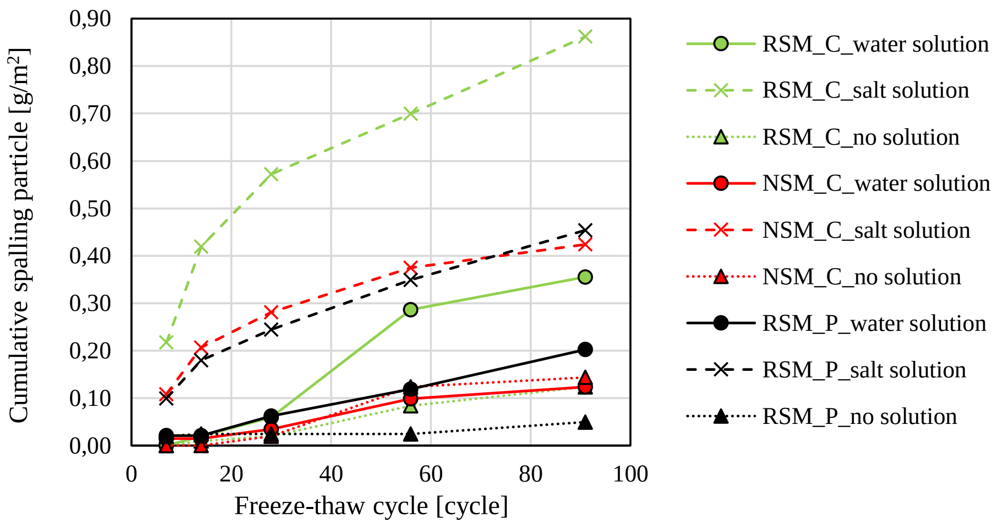

(a)

(b)

[1 kg/m^2 = 0.2048 lb/ft^2]

Fig. 14—Cumulative spalling particles of cast and printed specimens submitted to different surface conditions during test (a), and surface conditions of RSM_P specimens after 91 freezing and thawing cycles (b) (1st row are the specimens with water solution, 2nd row are the specimens with salt solution, and 3rd row are the specimens with no solution)